Thermodynamic assessment of the oxygen reduction activity in aqueous solutions

Tripkovic, Vladimir

Published in:
Physical Chemistry Chemical Physics

Link to article, DOI:
10.1039/c7cp05448c

Publication date:
2017

Document Version
Peer reviewed version

Thermodynamic assessment of the oxygen reduction activity in aqueous solutions

Vladimir Tripkovic[1]

[1] Department of Energy Conversion and Storage, Technical University of Denmark, DK-2800 Kgs. Lyngby, Denmark.

In the conventional theoretical approach, oxygen reduction reaction activities are assessed through a volcano plot using activity descriptors. The volcano plot resides on several approximations, e.g. the reaction kinetics is commonly overlooked and the interaction of hydrophilic intermediates with water is considered constant regardless of the metal surface. Herein, we demonstrate by means of density functional theory calculations that the binding energies of hydrophilic intermediates are strongly influenced by hydrogen bonding (HB) to surface water molecules. We find the HB energies of adsorbed OOH and OH on a number of active metallic (strained and non-strained Pt, Pd, Ag) and bimetallic (Pt_3Ni, Pt_3Co, PtCu, Pd@Pt-skin and Pt@Pd-skin) 111 surfaces to vary by up to 0.5 eV in energy. Furthermore, we show that the existence of a universal scaling line is a relative notion, contingent on the accuracy of the results. Scaling errors can be reduced substantially by partitioning data into subsets depending on the element comprising the surface layer. Finally, the activity volcano that explicitly includes HB and van der Waals interactions reproduces the right experimental trend for Pt and its alloys, but at the same time predicts Ag to be a more active catalyst than Pt. The latter result is explained by assuming the same water structure at the surface and the fact that reaction kinetics is neglected.

Keywords: oxygen reduction reaction, density functional theory, hydrogen bonding, volcano, scaling relations, Pt, alloys.

1. Introduction

The oxygen reduction reaction (ORR) is perhaps the most vital electro-catalytic reaction of our time.[1–3] Its importance lies in the fact that it enters in many electrochemical conversion devices (fuel cells, metal-air batteries, in the electrochemical production of hydrogen peroxide and chlorine etc.) that are envisaged to play a major role in transformation from carbon-based to carbon-free society. What still prevents the deployment of these technologies is the sluggishness of the ORR.[4,5] A new insight provided by theoretical calculations has laid foundations for quickly assessing

activities of potential catalysts.[6] The theoretical insight hinges on linear scaling relations that exist between adsorption energies of reaction intermediates.[7–9] According to this concept, the number of unknowns in a system is essentially given by the number of intermediates in the reaction path. As the binding energies (BEs) of different intermediates mutually scale, the number of unknowns can be reduced to one, or at most two depending on reaction.[6,9] The scaling relations give rise to volcano plots, in which a chosen BE is used as an activity estimation parameter, i.e. activity descriptor.[9] Relating activity to easily computable BEs opened up a route for fast screening of many catalytic materials for the ORR,[10–14] and other reactions.[9,15–18] In addition, the scaling relations have been used to assess the structure-activity relationships of different facets.[19,20] However, this simple model is based on several approximations, e.g. the interaction of water with surface intermediates is treated approximatively (*vide supra*), while the kinetics are commonly disregarded. For catalysts with optimal BEs that lie close to the top of the volcano, theoretical activity predictions give much higher rates compared to experimentally measured activities.[11] The offset has been explained by the fact that reaction kinetics become important close to the volcano top.[21] In this study we evaluate the accuracy of the ORR volcano, and discuss whether activity predictions can be related to reaction thermochemistry alone or kinetic contributions must be taken into account as well.

The ORR involves hydrophilic OH and OOH intermediates that are stabilized by vicinal water molecules through HB. In the standard volcano approach, the influence of water on adsorption energy is assumed constant.[8,10,11] Here, we demonstrate how HB can stabilize OH and OOH intermediates by as much as 0.5 eV depending on the metal surface. Furthermore, we show how the inclusion of HB energies affects scaling relations and volcano plots that are derived from these.

2. Method

Total energies of different surfaces with adsorbates are calculated using Density Functional Theory (DFT) calculations employing the grid-based projector-augmented wave method (GPAW) code integrated with Atomic Simulation Environment (ASE).[22] Calculations are performed using the RPBE exchange-correlation functional.[23] Occupation of one-electron states is calculated at an electronic temperature of k_BT = 0.1 eV, and then all energies are extrapolated to k_BT = 0 K.

Metal electrodes are represented by periodically repeated slabs separated by at least 10 Å of vacuum. Three unit cell sizes are used to simulate the (111) and (0001) close-packed surfaces of the metals and alloys with 2x2, 3x2 and 3x3 atoms in the surface plane. For the three cells we used the

4x4x1, 4x6x1 and 4x4x1 Monkhorst–Pack k-point sampling grids,[24] respectively. Atoms in the two bottom layers are fixed to bulk distances, while the remaining atoms and adsorbates are allowed to relax in order to assume minimum energy positions. The convergence is reached when the sum of absolute forces becomes less than 0.05 eVÅ^{-1}. Pt@Pd-skin, Pd@Pt-skin and PtCu- near-surface alloys (NSA) have the lattice constant of the host metal, in which the surface layer in Pt@Pd-skin and Pd@Pt-skin, and the subsurface layer in the NSA are substituted by solute atoms. The $Pt_3Ni(111)$ and $Pt_3Co(111)$ surfaces were modeled having a Pt skin and an enriched 50% content of Ni and Co in the second layer as found in Refs. 10 and 25. Spin-polarized calculations have been employed for alloys containing Co and Ni. It is noteworthy stressing that these calculations have been performed with a very narrow 0.15 Å grid spacing and relatively thick metal slabs, which is at the limit of the system size and computational accuracy that can be achieved at the moment.

Ordering of water at the metal/water interfaces has not been elucidated even for seemingly simple close-packed surfaces. It is practically impossible to experimentally probe the surface water layer under ambient conditions due to difficulty in distinguishing between vibrational modes of the interfacial and liquid water. In most cases, water wetting patterns are taken from UHV studies at mono- or submonolayer coverages. Nevertheless, even under these conditions a rich complexity of water structures is observed, including complete and dissociated water layers.[26,27] For the purpose of modelling the metal/aqueous interfaces, we will use a well-known water bilayer structure observed on Pt(111) in UHV studies.[28] It is important to note that ordering of water will likely be different for the different transition metals.[27,29] In fact, even for the same surface, an ensemble of different configurations similar in energy will be simultaneously present on the surface. Given the lack of experimental results, water bilayer is a representative structure for water organization at metal/water interfaces. It has been also used extensively in other computational modelling studies.[29–36] Different coverages of OH and OOH in water bilayer are modelled by replacing water molecules with dangling hydrogen bonds with the OH and OOH moieties (see Note 1 in the Electronic Supplementary Information, ESI) using the approach in ref. [37] and assuming that water at the surface is in equilibrium with liquid water.[35,36,38] The HB energies of OH and OOH, ΔE_{OH}^{HB} and ΔE_{OOH}^{HB}, are calculated through equations (1) - (4):

$$\Delta E^{\text{int}}_{OH^{bl}/OOH^{bl}}(x) = E\left[slab + (\frac{2}{3}N - x)H_2O + x(OH/OOH)\right] - (\frac{2}{3}N - x)\cdot E(H_2O^{bl}) - (x+z)\cdot E(H_2O) + (\frac{x}{2}+z)\cdot E(H_2) \quad (1)$$

$$\Delta E^{diff}_{OH^{bl}/OOH^{bl}}(x) = E\left[slab + (\frac{2}{3}N - x - 1)H_2O + (x+1)(OH/OOH)\right] - E\left[slab + (\frac{2}{3}N - x)H_2O + x(OH/OOH)\right] + \Delta E(H_2O^{bl}) - E(H_2O) + E(H_2) \quad (2)$$

$$\Delta E(H_2O^{bl}) = \left\{E\left[slab + \frac{2}{3}N\cdot H_2O)\right] - E(slab)\right\} / \frac{2}{3}N \quad (3)$$

$$\Delta E^{HB}_{OH} = \Delta E^{diff}_{OH^{bl}} - \Delta E^{dry}_{OH},\ \Delta E^{HB}_{OOH} = \Delta E^{diff}_{OOH^{bl}} - \Delta E^{dry}_{OOH}, \quad (4)$$

where $\Delta E^{\text{int}}_{OH^{bl}}$ and $\Delta E^{diff}_{OH^{bl}}$ are the integral and the differential binding energies of OH and OOH in the bilayer,[1] ΔE^{dry}_{OH} and ΔE^{dry}_{OOH} are the BEs of OH and OOH on top of a metal atom in the absence of water. In the case of Ag(111), ΔE^{dry}_{OH} and ΔE^{dry}_{OOH} are calculated for OH and OOH on a bridge site because they were not found to be stable at the top site. *x* and *2/3N-x* are the numbers of OH/OOH species and co-adsorbed water molecules, respectively. The differential binding energies have been calculated on the 3x3 surface for which x = 0 – 2 (cf. Figure S1 and S2 in Note 1 in the Electronic Supplementary Information, ESI). *Z* is a parameter that assumes zero value for OH and one for OOH. The BE of a water molecule in water bilayer, $E(H_2O^{bl})$, is calculated *via* Eq. (3) and is largely material independent.[39] The HB energies are calculated through Eq. (4) by comparing the BEs of non-hydrated, henceforth 'dry' and hydrated, henceforth 'wet' intermediates. Volcano plots are derived using the approach outlined in refs 6 and 40. For calculating BEs we used liquid H_2O and gas phase H_2 as references and the corresponding zero-point energy and entropy corrections.[6] Electric field effects have been omitted because they were shown to have a minor effect on the OH and essentially no effect on the OOH BE.[37,41] ORR activities are calculated at standard conditions (k_BT = 0.0257 eV) using the Arrhenius law and a prefactor of 10^{13} s^{-1}.

[1] bl abbreviation stands for water bilayer

3. Results and discussion

We have systematically analyzed HB energies on pristine and strained Pt(111), Pd(111), Ag(111) and several alloy surfaces (Pt_3Ni, Pt_3Co, Pd@Pt-skin, Pt@Pd-skin and PtCu NSA) with the (111) termination. The selected subset included all the active catalysts for the ORR,[11,13,42,43] in which the activity is controlled by the nature of the material, strain and/or ligand effect. This careful chosen subset makes it possible to assess the influence of each effect individually on the ORR activity. The strain is varied from the -2% tensile to the +5% compressive strain on Pt(111) and Pd(111), and from the -2% compressive to the +5% tensile strain on Ag(111). The different amount of applied strain is rationalized by the positions of Pt(111), Pd(111) and Ag(111) on the conventional ORR volcano.[6] As Pt(111) and Pd(111) are located on the left volcano leg, a slight reduction in BE due to compressive strain should in principle promote the ORR activity. In contrast, Ag(111) sits on the right volcano leg. Imposing a tensile strain on the Ag(111) surface should increases the OH BE resulting in higher ORR activities. For Pt(111), we show results under tensile strain only. We have noticed that under compressive strain in the presence of a mixed OH and H_2O adlayer, the platinum slab reconstructs and the surface layers lose the cubic close-packing arrangement. The reconstruction sets in already at ca. 1% strain. In addition to strain effect, we have also studied ligand effect by considering some of the most active Pt alloys. On Pt_3Ni and Pt_3Co ligand effect is convoluted with strain effect. The pure ligand effect can however be discerned on the PtCu NSA, which has the lattice constant of Pt, implying that the topmost Pt layer is under the influence of ligand effect from subsurface Cu only. We will use activities of the alloys and the pristine metals to evaluate how accurately ORR estimates can be made with the thermodynamic volcano plot.

In the conventional approach, the effect of the water solvent on the OH and OOH BEs is calculated on Pt(111) and then the same corrections are used for all other (111) transition metal surfaces.[6,8] Herein, we have calculated the HB energies of OH and OOH with water for every investigated surface separately (cf. **Figure 1**). HB energies were computed through Eq. (4), which compares Bes of the dry and wet OH/OOH. For the hydrophobic O intermediate we assume that water has negligible effect on the activity.[8,34]

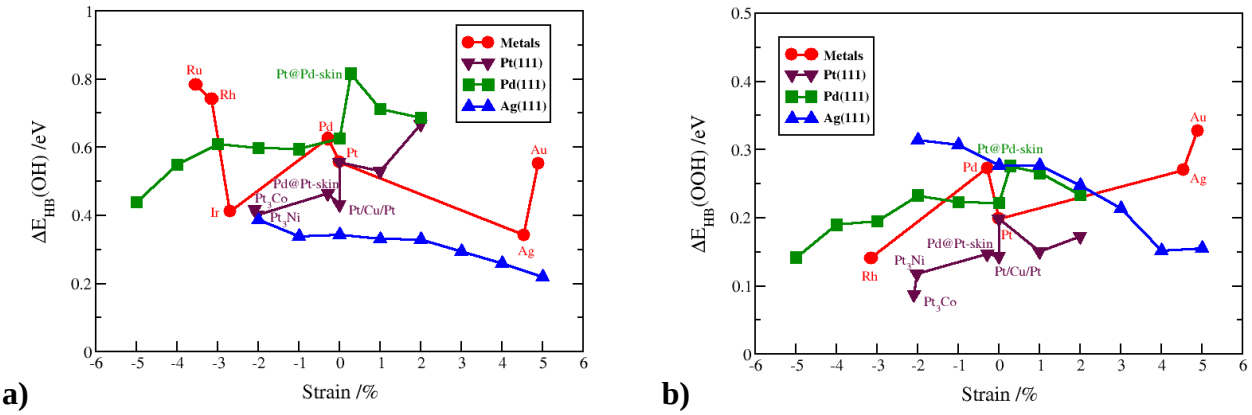

Figure 1 Hydrogen bonding energies for a) OH and b) OOH represented on a strain scale. For metals and alloys strain is measured compared to the Pt lattice.

What is striking at first glance is that HB energies are strongly dependent on the catalyst surface. The difference in HB energies across different catalysts is approximately two times higher for the OH than the OOH species. The maximum difference (0.5 eV for OH and 0.3 eV for OOH) is discerned for transition metals. We further notice that HB energies are dependent on the strain and ligand effect, such that for the strained Pt(111), Pd(111) and Ag(111) surfaces, the value varies by 0.2 - 0.3 eV, whereas for the PtCu NSA the variation is 0.18 eV.

In the following analysis, we demonstrate how HB energies affect ORR activities assessed from the volcano plot. The scaling relations for dry and wet intermediates are presented in **Figure 2** (BEs are listed in Note 2 in the ESI). In addition, Mean Absolute Errors (MAE) and standard deviations (σ) are summarized in **Table 1**.

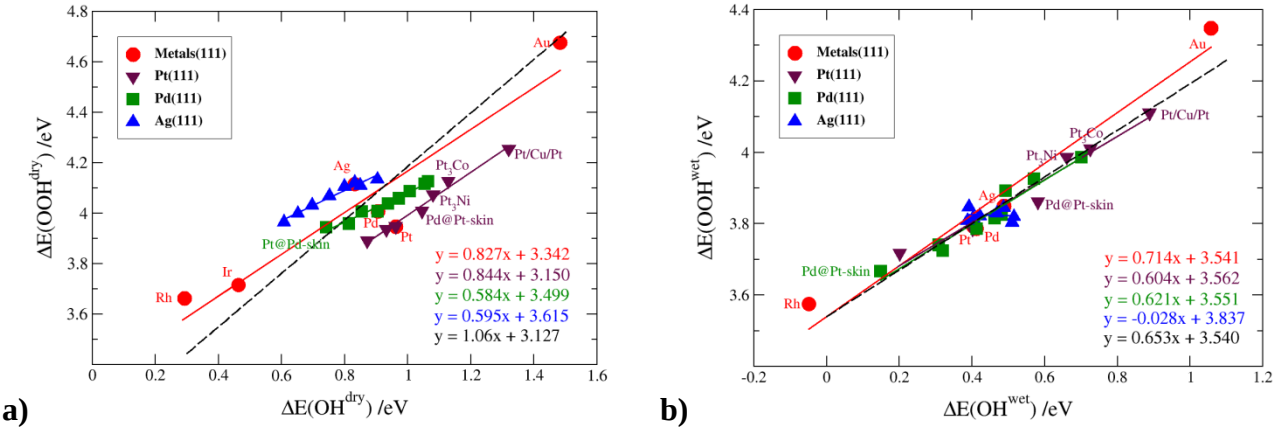

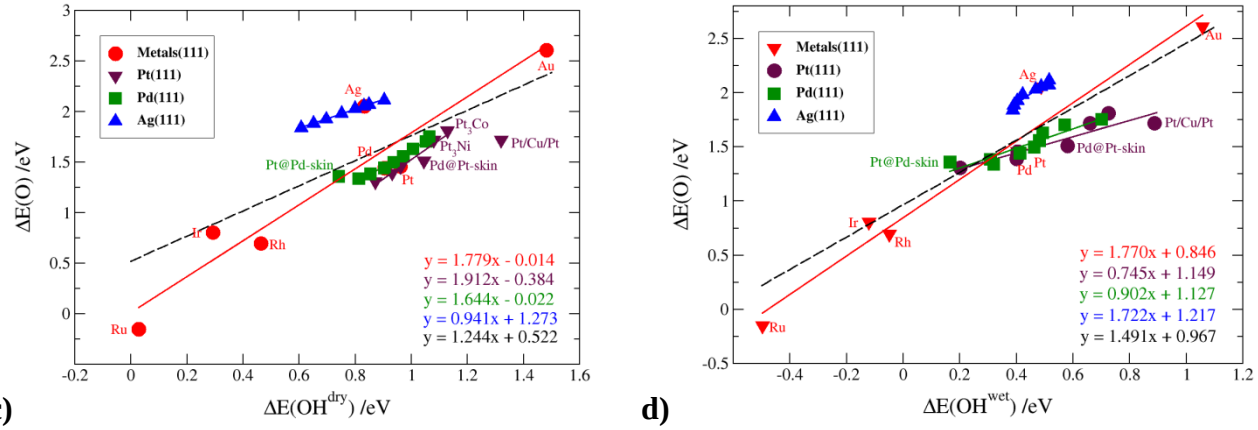

Figure 2 Scaling relationships for dry a) and c), and wet b) and d) intermediates. Linear fits for catalysts terminating with the Pt, Pd, Ag layer are denoted by maroon, green and blue lines, respectively. Universal scaling relations are denoted by dashed black lines.

Table 1 Mean absolute errors for surface specific and universal scaling lines. Standard deviations are also shown for comparison separated by '/' for universal fits. Values are given in units of eVs.

	Metals(111)	Pt(111)	Pd(111)	Ag(111)	Universal fit
OOH vs OH dry	0.092	0.013	0.009	0.001	0.130/0.146
OOH vs OH wet	0.049	0.023	0.024	0.012	0.028/0.038
O vs OH dry	0.239	0.035	0.036	0.020	0.316/0.361
O vs OH wet	0.149	0.062	0.045	0.020	0.223/0.261

Results in **Figure 2** and **Table 1** are used to draw several important conclusions.

1. MAEs or σ should be used as figures of merit when evaluating scaling relationships. As can be seen, the MAEs are smaller for wet than dry intermediates. The scaling errors are also smaller for the OH vs. OOH BE fits than when OH and OOH are scaled against the O BE, individually. This is explained by the fact that both OH and OOH adsorb at the same surface site (bridge for Ag and top for all the other catalysts), whereas O prefers three-fold coordinated sites.
2. Fitting all the points with a single scaling line leads to large MAEs and σs, except for the OOH vs. OH BE fit for wet intermediates. In contrast, catalysts (strained metals and alloys) that terminate with the same surface layer produce much better correlations. Surfaces

terminating with Pt(111) or Pd(111) follow nearly the same trends, whereby those terminating with Ag(111) are considerably off, most likely due to differences in the lattice constants between Pt(111) and Pd(111) on one and Ag(111) on the other side.

3. It is noteworthy that the slopes and intercepts of the scaling relations vary significantly from one dataset to another. Moreover, the slopes do not always follow a simple bond counting rule, according to which the scaling of the O vs. OH and OOH vs. OH BEs have a slope of 2 and 1, respectively. Herein, we find the slopes to fluctuate between 0.7 and 2 for former, and between 0 and 1 for the latter fit.
4. The slopes and intercepts are sensitive to the number of points and the weight of each point. Therefore, including more points in the fits, especially terminal points, might cause the slopes and intercepts to change. In the optimum BE range corresponding to the top of the volcano, the precision should be very high given the large number of points. In fact, including more points outside of the optimal region can make MAE and σ worse.

As the scaling relationships give rise to volcano plots, any change in the slope and/or intercept will automatically reflect on the appearance of the volcano. The thermodynamic volcano is derived from the differences in binding free energies of reaction intermediates through reactions: [6,40]

$$\Delta G_1 = \Delta E_{OH} - \Delta E_{H2O} + C1 \quad (5)$$

$$\Delta G_2 = \Delta E_{O} - \Delta E_{OH} + C2 \quad (6)$$

$$\Delta G_3 = \Delta E_{OOH} - \Delta E_{O} + C3 \quad (7)$$

$$\Delta G_4 = \Delta E_{O_2} - \Delta E_{OOH} + C4 \quad (8)$$

using the Computational Standard Hydrogen Electrode approach,[6] which assumes coupled proton-electron transfer steps. ΔEs are the BEs of different intermediates, ΔE_{H2O} and ΔE_{O_2} are usually taken as constants assuming that neither H_2O(l) nor O_2(g) adsorb to the surface. C1 - C4 are the zero point energy and entropy corrections for 4 electrochemical steps.[6,40] According to the ORR volcano, ΔG_1 or ΔG_4 is a Potential Determining Step (PDS), i.e. the step with the highest thermodynamic barrier for reaction.[8,44] If ΔE_{OH} is chosen as activity descriptor, the left volcano leg ΔG_1 has a slope of 1 and an intercept of C1. The one-to-one mapping between the first electrochemical step and activity descriptor cancels out the scaling errors. ΔG_4, which describes the right volcano leg depends on the ΔE_{OOH}, which in turn can be related to the OH BE through a linear

scaling relationship. The BEs of OH and OOH were previously shown to scale linearly with a slope 1 and an intercept of 3.2 ± 0.2 eV on a range of different transition metal and oxide surfaces.[45] Contrary to ΔG_1 there is no such error cancelation for ΔG_4. Hence, the scaling errors are present at the right volcano leg.[46] If oxygen is taken as activity descriptor instead, then the errors are present at both volcano legs because both ΔG_1 and ΔG_4 have to be defined in terms of the O BE. In cases when scaling errors enter into the PDS, the uncertainty in rate is given by the Arrhenius expression:

$$\Delta r = e^{(MAE/\sigma)/k_B T} \qquad (9)$$

As a rule of thumb for every 0.06 eV change in the PDS, the activity changes by an order of magnitude. With an error of 0.2 eV in the scaling of the OH vs OOH BEs corresponding roughly to 10^3 difference in activity, it is not possible to ascertain whether a catalyst situated on the right volcano leg, that binds intermediates somewhat more weakly, is a more active catalyst than Pt. In such situations it is better to have a scaling relationship for every subset comprising catalysts that terminate with the same layer.

Volcano plots derived from scaling relations for wet intermediates are shown in **Figure 3** using both the O and OH BE as activity descriptor. The most important metal and alloy points (Pt, Pd, Ag, Pt_3Ni and Pt_3Co) are indicated and used as benchmarks for evaluating the accuracy of activity predictions.

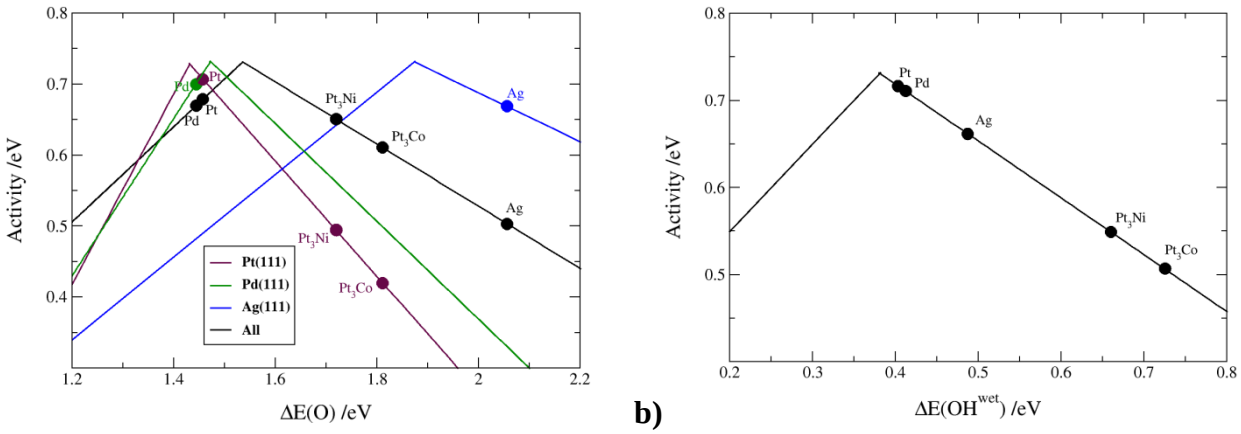

Figure 3 Volcano plots for oxygen reduction for wet intermediates using the a) O and b) OH binding energy as activity descriptor. Hydrogen bonding energies with water are explicitly included for every surface. The (111) symbols are omitted for clarity. The black filled circles in a) are projections onto a universal scaling line.

According to **Figure 3**a, the surfaces of strained metals and alloys terminating with a Pt(111), Pd(111) or Ag(111) layer follow different trends. For instance, all the catalysts with the Pt(111) surface layer (Pt, Pt_3Ni, Pt_3Co, PtCu NSA and Pd@Pt-skin) fall on the same volcano plot. Arranging data into distinct subsets gives rise to multiple volcano plots, where each volcano describes activities of that particular subset more accurately. The errors in predicted activities are given by vertical projections of points from specific to a universal scaling line. Using the OH BE as activity descriptor causes all the points to collapse to a single scaling line (cf. **Figure 3**b). At this point it should be noted that there is no such notion as absolute scaling relationship or volcano plot. Having multiple or a single scaling line and volcano plot is contingent upon how large errors in activity predictions can be tolerated. For the right volcano leg in Figure 3b we get a very small MAE/σ value of 0.028/0.038 eV, resulting in the 3 - 4 times difference in the ORR activity only. A similar effect of water on the OOH and OH BEs was recently reported for metalloporphyrins.[47] Even with the correct inclusion of the HB energies, **Figure 3**b fails to describe the experimental activity trend for the benchmark electrocatalysts. It produces the good activity order for pristine metals: Pt(111) > Pd(111) > Ag(111), but erroneously predicts activities of the Pt alloys to be lower than that of Pt. One of the reasons why **Figure 3**b fails to capture the observed experimental trend might be because van der Waals (vdW) interactions have not been taken into account. Adding the vdW corrections accounted by the Tkatchenko−Scheffler method,[48] on top of the RPBE or PBE XC functional stabilized the OH and OOH BEs by an additional 0.15 and 0.25 eV, respectively.[49] Accordingly, including vdW interactions shifts the right volcano leg to the right by 0.1 eV, while at the same time the $\Delta E(OH^{wet})$ reduces by 0.15 eV (cf. **Figure 4**).

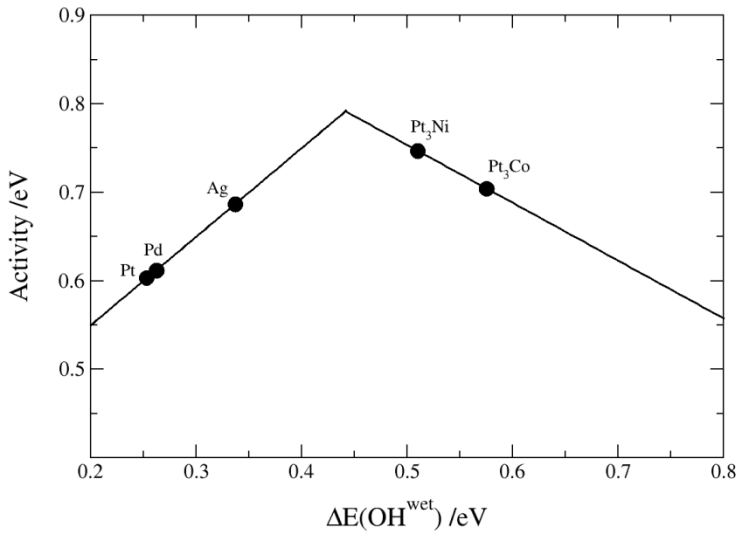

Figure 4 Volcano plot for wet intermediates including corrections for van der Waals interactions.

As seen, **Figure 4** describes the activity trend of Pt, Pt_3Ni and Pt_3Co much better than **Figure 3**b. However, it still displays two inconsistencies compared to experiments: 1) Pd is slightly more active than Pt and 2) Ag is far more active than Pt or Pd. Pt and Pd exhibit similar activities experimentally[50,51] suggesting that it will be hard to distinguish between them at the DFT level. As we see it, there are two reasons for the observed deviation in the case of Ag(111): 1) the conjecture that water adsorbs in the same configuration on all the surface and 2) the fact that kinetic effects are neglected. Regarding the first argument, the effect of HB was estimated assuming the fixed water bilayer structure. While the same ordering of water can be expected for Pd, Pt and the active alloys due to small differences in the lattice constants, there is no such argument to support the use of water bilayer on Ag(111). In fact, it was demonstrated in MD studies that water on Ag(111) is ordered differently than on Pt(111).[29,53] Another result that points implicitly to different organization of water at the interface are the different adsorption sites for dry OH and OOH on Ag(111) and other catalysts. Regarding the second argument, the wrong activity estimates in **Figure 4** can also originate from surface-sensitive barriers for breaking the O-O bond. This hypothesis is substantiated by the existence of well-known linear correlations between the dissociation energies and reaction enthalpies better known as the Brønsted-Evans-Polanyi relationships.[54,55] The computed O_2 dissociation barrier is much higher,[34,56–58] whereas the sticking coefficient, inferred from UHV experiments, is much lower on Ag(111) than on Pt(111).[59–61]

Finally, it should be mentioned that in an alternative interpretation, the errors in scaling relations were assigned to errors in the XC functional. It was demonstrated using a large ensemble of XC functionals that DFT calculations cannot give absolute activity predictions, but can predict activity only with a certain probability measured by standard deviation, σ. For the OOH vs OH BE scaling relationship, σ = 0.18 eV,[46] which is 0.14 eV higher than the value calculated herein employing one particular XC functional.

4. Conclusions

Herein, we presented a comprehensive thermodynamic analysis of the ORR activity from first principles calculations. A major difference compared to previous studies is that the HB energies of

OH and OOH are not assumed constant, but calculated separately for each and every system under study. The most important conclusions are summarized in the following points:

1. HB energies are strongly dependent on the metal surface, strain and ligand effect.
2. ORR activity estimates are extremely sensitive on the linear fitting. In principle, the fitting should be performed such that it minimizes MAEs or σ, because a small change in the BE can bring about a large error in activity prediction.
3. The OH BE is a better activity descriptor than the O BE.
4. Universality in scaling relationships and volcano plots is a relative notion that depends on how accurate results one can accept.
5. Explicitly including the HB energies in the case of wet intermediates minimizes significantly the scaling errors at the right volcano leg.
6. Even after partitioning data into subsets and appropriate inclusion of the HB energies, the resulting volcanos failed to describe the relative activity order of Pt and its alloys.
7. Inclusion of vdW corrections produces the right activity trend, but erroneously predicts Ag to be far more active than Pt. This is either because of a different water structure on Ag(111) or the fact that kinetic effects have not been considered.

We believe that many aspects of this study can be generalized to other (electro)chemical reactions, where scaling relations and volcano plots are used as activity estimation tools. Results presented here call for a more detailed study of kinetic effects, including accurate estimations of the O-O breaking, charge transfer barriers and quantification of the length-scale of processes occurring at the metal/aqueous interfaces.

Conflict of interest

The authors declare no competing financial interest.

Abbreviations

ORR, Oxygen Reduction Reaction; PDS, Potential Determining Step; HB, hydrogen bonding; BE, binding energy, near-surface alloy (NSA).

References

1 G. M. Whitesides and G. W. Crabtree, Don’t forget long-term fundamental research in

energy., *Science*, 2007, **315**, 796–8.

2 B. C. Steele and A. Heinzel, Materials for fuel-cell technologies., *Nature*, 2001, **414**, 345–52.

3 M. K. Debe, Electrocatalyst approaches and challenges for automotive fuel cells., *Nature*, 2012, **486**, 43–51.

4 H. A. Gasteiger, S. S. Kocha, B. Sompalli and F. T. Wagner, Activity benchmarks and requirements for Pt, Pt-alloy, and non-Pt oxygen reduction catalysts for PEMFCs, *Appl. Catal. B-Environmental*, 2005, **56**, 9–35.

5 N. Markovic, H. Gasteiger and P. N. Ross, Kinetics of oxygen reduction on Pt(hkl) electrodes: Implications for the crystallite size effect with supported Pt electrocatalysts, *J. Electrochem. Soc.*, 1997, **144**, 1591–1597.

6 J. K. Nørskov, J. Rossmeisl, A. Logadottir, L. Lindqvist, J. R. Kitchin, T. Bligaard and H. Jonsson, Origin of the overpotential for oxygen reduction at a fuel-cell cathode, *J. Phys. Chem. B*, 2004, **108**, 17886–17892.

7 F. Abild-Pedersen, J. Greeley, F. Studt, J. Rossmeisl, T. R. Munter, P. G. Moses, E. Skulason, T. Bligaard and J. K. Nørskov, Scaling properties of adsorption energies for hydrogen-containing molecules on transition-metal surfaces, *Phys. Rev. Lett.*, 2007, **99**, 1–4.

8 J. Rossmeisl, A. Logadottir and J. K. Nørskov, Electrolysis of water on (oxidized) metal surfaces, *Chem. Phys.*, 2005, **319**, 178–184.

9 J. K. Nørskov, T. Bligaard, J. Rossmeisl and C. H. Christensen, Towards the computational design of solid catalysts, *Nat. Chem.*, 2009, **1**, 37–46.

10 J. Greeley, I. E. L. Stephens, A. S. Bondarenko, T. P. Johansson, H. A. Hansen, T. F. Jaramillo, J. Rossmeisl, I. Chorkendorff and J. K. Nørskov, Alloys of platinum and early transition metals as oxygen reduction electrocatalysts, *Nat. Chem.*, 2009, **1**, 552–556.

11 I. E. L. Stephens, A. S. Bondarenko, F. J. Pérez-Alonso, F. Calle-Vallejo, L. Bech, T. P. Johansson, A. K. Jepsen, R. Frydendal, B. P. Knudsen, J. Rossmeisl and I. Chorkendorff, Tuning the Activity of Pt(111) for Oxygen Electroreduction by Subsurface Alloying, *J. Am. Chem. Soc.*, 2011, **133**, 5485–5491.

12 I. E. L. Stephens, A. S. Bondarenko, U. Grønbjerg, J. Rossmeisl and I. Chorkendorff, Understanding the electrocatalysis of oxygen reduction on platinum and its alloys, *Energy Environ. Sci.*, 2012, **5**, 6744–6762.

13 R. R. Adzic, J. Zhang, K. Sasaki, M. B. Vukmirovic, M. Shao, J. X. Wang, A. U. Nilekar, M. Mavrikakis, J. A. Valerio and F. Uribe, Platinum monolayer fuel cell electrocatalysts, *Top. Catal.*, 2007, **46**, 249–262.

14 F. Calle-Vallejo, J. I. Martinez and J. Rossmeisl, Density functional studies of functionalized graphitic materials with late transition metals for oxygen reduction reactions, *Phys. Chem. Chem. Phys.*, 2011, **13**, 15639–15643.

15 J. Greeley, T. F. Jaramillo, J. Bonde, I. B. Chorkendorff and J. K. Nørskov, Computational high-throughput screening of electrocatalytic materials for hydrogen evolution, *Nat. Mater.*, 2006, **5**, 909–913.

16 E. Skulason, T. Bligaard, S. Gudmundsdottir, F. Studt, J. Rossmeisl, F. Abild-Pedersen, T. Vegge, H. Jonsson and J. K. Nørskov, A theoretical evaluation of possible transition metal electro-catalysts for N-2 reduction, *Phys. Chem. Chem. Phys.*, 2012, **14**, 1235–1245.

17 V. Tripkovic, M. Vanin, M. Karamad, M. E. Björketun, K. W. Jacobsen, K. S. Thygesen and J. Rossmeisl, Electrochemical CO 2 and CO Reduction on Metal-Functionalized Porphyrin-like Graphene, *J. Phys. Chem. C*, 2013, **117**, 9187–9195.

18 E. M. Fernandez, P. G. Moses, A. Toftelund, H. A. Hansen, J. I. Martinez, F. Abild-Pedersen, J. Kleis, B. Hinnemann, J. Rossmeisl, T. Bligaard and J. K. Nørskov, Scaling relationships for adsorption energies on transition metal oxide, sulfide, and nitride surfaces, *Angew. Chemie-International Ed.*, 2008, **47**, 4683–4686.

19 F. Calle-Vallejo, D. Loffreda, M. T. M. Koper and P. Sautet, Introducing structural sensitivity into adsorption–energy scaling relations by means of coordination numbers, *Nat. Chem.*, 2015, **7**, 403–410.

20 F. Calle-Vallejo, J. Tymoczko, V. Colic, Q. H. Vu, M. D. Pohl, K. Morgenstern, D. Loffreda, P. Sautet, W. Schuhmann and A. S. Bandarenka, Finding optimal surface sites on heterogeneous catalysts by counting nearest neighbors, *Science (80-.).*, 2015, **350**, 185–189.

21 V. Viswanathan and H. A. Hansen, Unifying Solution and Surface Electrochemistry: Limitations and Opportunities in Surface Electrocatalysis, *Top. Catal.*, 2013, **57**, 215–221.

22 J. Mortensen, L. Hansen and K. Jacobsen, Real-space grid implementation of the projector augmented wave method, *Phys. Rev. B*, 2005, **71**, 1–11.

23 B. Hammer, L. Hansen and J. Nørskov, Improved adsorption energetics within density-

functional theory using revised Perdew-Burke-Ernzerhof functionals, *Phys. Rev. B*, 1999, **59**, 7413–7421.

24 H. J. Monkhorst, Special points for Brillouin-zone integrations, *Phys. Rev. B*, 1976, **13**, 5188–5192.

25 V. R. Stamenkovic, B. S. Mun, M. Arenz, K. J. J. Mayrhofer, C. A. Lucas, G. F. Wang, P. N. Ross and N. M. Markovic, Trends in electrocatalysis on extended and nanoscale Pt-bimetallic alloy surfaces, *Nat. Mater.*, 2007, **6**, 241–247.

26 S. Nie, P. J. Feibelman, N. C. Bartelt and K. Thürmer, Pentagons and Heptagons in the First Water Layer on Pt(111), *Phys. Rev. Lett.*, 2010, **105**, 26102.

27 J. Carrasco, A. Hodgson and A. Michaelides, A molecular perspective of water at metal interfaces, *Nat. Mater.*, 2012, **11**, 667–674.

28 C. Clay, S. Haq and A. Hodgson, Hydrogen bonding in mixed OH+H2O overlayers on Pt(111), *Phys. Rev. Lett.*, 2004, **92**, 46102.

29 S. Schnur and A. Groß, Properties of metal–water interfaces studied from first principles, *New J. Phys.*, 2009, **11**, 125003.

30 E. Skulason, V. Tripkovic, M. E. Bjorketun, S. Gudmundsdottir, G. Karlberg, J. Rossmeisl, T. Bligaard, H. Jonsson and J. K. Nørskov, Modeling the Electrochemical Hydrogen Oxidation and Evolution Reactions on the Basis of Density Functional Theory Calculations, *J. Phys. Chem. C*, 2010, **114**, 18182–18197.

31 V. Tripkovic, M. Björketun, E. Skúlason and J. Rossmeisl, Standard hydrogen electrode and potential of zero charge in density functional calculations, *Phys. Rev. B*, 2011, **84**, 1–11.

32 J. Rossmeisl, K. Chan, R. Ahmed, V. Tripkovic and M. E. Bjorketun, pH in atomic scale simulations of electrochemical interfaces, *Phys. Chem. Chem. Phys.*, 2013, **15**, 10321–10325.

33 W. Tang, H. F. Lin, A. Kleiman-Shwarsctein, G. D. Stucky and E. W. McFarland, Size-dependent activity of gold nanoparticles for oxygen electroreduction in alkaline electrolyte, *J. Phys. Chem. C*, 2008, **112**, 10515–10519.

34 S. Liu, M. G. White and P. Liu, Mechanism of Oxygen Reduction Reaction on Pt(111) in Alkaline Solution: Importance of Chemisorbed Water on Surface, *J. Phys. Chem. C*, 2016, **120**, 15288–15298.

35 A. B. Anderson, R. Jinnouchi and J. Uddin, Effective Reversible Potentials and Onset Potentials for O $_2$ Electroreduction on Transition Metal Electrodes: Theoretical Analysis, *J. Phys. Chem. C*, 2013, **117**, 41–48.

36 J. Rossmeisl, K. Chan, E. Skúlason, M. E. Björketun and V. Tripkovic, On the pH dependence of electrochemical proton transfer barriers, *Catal. Today*, 2016, **262**, 36–40.

37 V. Tripkovic, E. Skúlason, S. Siahrostami, J. K. Nørskov and J. Rossmeisl, The oxygen reduction reaction mechanism on Pt(1 1 1) from density functional theory calculations, *Electrochim. Acta*, 2010, **55**, 7975–7981.

38 J. Rossmeisl, E. Skúlason, M. E. Björketun, V. Tripkovic and J. K. Nørskov, Modeling the electrified solid–liquid interface, *Chem. Phys. Lett.*, 2008, **466**, 68–71.

39 A. Michaelides, A. Alavi and D. King, Insight into H2O-ice adsorption and dissociation on metal surfaces from first-principles simulations, *Phys. Rev. B*, 2004, **69**, 113404.

40 J. Rossmeisl, Z. W. Qu, H. Zhu, G. J. Kroes and J. K. Nørskov, Electrolysis of water on oxide surfaces, *J. Electroanal. Chem.*, 2007, **607**, 83–89.

41 G. S. Karlberg, J. Rossmeisl and J. K. Nørskov, Estimations of electric field effects on the oxygen reduction reaction based on the density functional theory, *Phys. Chem. Chem. Phys.*, 2007, **9**, 5158–5161.

42 V. R. Stamenkovic, B. Fowler, B. S. Mun, G. F. Wang, P. N. Ross, C. A. Lucas and N. M. Markovic, Improved oxygen reduction activity on Pt3Ni(111) via increased surface site availability, *Science (80-.).*, 2007, **315**, 493–497.

43 S. Mukerjee and S. Srinivasan, ENHANCED ELECTROCATALYSIS OF OXYGEN REDUCTION ON PLATINUM ALLOYS IN PROTON-EXCHANGE MEMBRANE FUEL-CELLS, *J. Electroanal. Chem.*, 1993, **357**, 201–224.

44 M. T. M. Koper, Thermodynamic theory of multi-electron transfer reactions: Implications for electrocatalysis, *J. Electroanal. Chem.*, 2011, **660**, 254–260.

45 I. C. Man, H.-Y. Su, F. Calle-Vallejo, H. A. Hansen, J. I. Martínez, N. G. Inoglu, J. Kitchin, T. F. Jaramillo, J. K. Nørskov and J. Rossmeisl, Universality in Oxygen Evolution Electrocatalysis on Oxide Surfaces, *ChemCatChem*, 2011, **3**, 1159–1165.

46 S. Deshpande, J. R. Kitchin and V. Viswanathan, Quantifying Uncertainty in Activity Volcano Relationships for Oxygen Reduction Reaction, *ACS Catal.*, 2016, **6**, 5251–5259.

47 F. Calle-Vallejo, A. Krabbe and J. M. García-Lastra, How covalence breaks adsorption-energy scaling relations and solvation restores them, *Chem. Sci.*, 2017, **8**, 124–130.

48 A. Tkatchenko and M. Scheffler, Accurate Molecular Van Der Waals Interactions from Ground-State Electron Density and Free-Atom Reference Data, *Phys. Rev. Lett.*, 2009, **102**, 73005.

49 R. Christensen, H. A. Hansen, C. F. Dickens, J. K. N?rskov and T. Vegge, Functional Independent Scaling Relation for ORR/OER Catalysts, *J. Phys. Chem. C*, 2016, **120**, 24910–24916.

50 X. Ge, A. Sumboja, D. Wuu, T. An, B. Li, F. W. T. Goh, T. S. A. Hor, Y. Zong and Z. Liu, Oxygen Reduction in Alkaline Media: From Mechanisms to Recent Advances of Catalysts, *ACS Catal.*, 2015, **5**, 4643–4667.

51 M. H. Shao, T. Huang, P. Liu, J. Zhang, K. Sasaki, M. B. Vukmirovic and R. R. Adzic, Palladium monolayer and palladium alloy electrocatalysts for oxygen reduction., *Langmuir*, 2006, **22**, 10409–15.

52 J. Gland, MOLECULAR AND ATOMIC ADSORPTION OF OXYGEN ON THE PT(111) AND PT(S)-12(111)X(111) SURFACES, *Surf. Sci.*, 1980, **93**, 487–514.

53 S. Izvekov and G. A. Voth, *Ab initio* molecular dynamics simulation of the Ag(111)-water interface, *J. Chem. Phys.*, 2001, **115**, 7196–7206.

54 A. Michaelides, Z.-P. Liu, C. J. Zhang, A. Alavi, D. A. King and P. Hu, Identification of general linear relationships between activation energies and enthalpy changes for dissociation reactions at surfaces., *J. Am. Chem. Soc.*, 2003, **125**, 3704–5.

55 J. K. Nørskov, T. Bligaard, A. Logadottir, S. Bahn, L. B. Hansen, M. Bollinger, H. Bengaard, B. Hammer, Z. Sljivancanin, M. Mavrikakis, Y. Xu, S. Dahl and C. J. H. Jacobsen, Universality in heterogeneous catalysis, *J. Catal.*, 2002, **209**, 275–278.

56 H.-Y. Su, M.-M. Yang, X.-H. Bao and W.-X. Li, The Effect of Water on the CO Oxidation on Ag(111) and Au(111) Surfaces: A First-Principle Study, *J. Phys. Chem. C*, 2008, **112**, 17303–17310.

57 Ye Xu, and Jeff Greeley and M. Mavrikakis*, Effect of Subsurface Oxygen on the Reactivity of the Ag(111) Surface, , DOI:10.1021/JA043727M.

58 D. J. Miller, H. Öberg, L.-Å. Näslund, T. Anniyev, H. Ogasawara, L. G. M. Pettersson and

A. Nilsson, Low O2 dissociation barrier on Pt(111) due to adsorbate-adsorbate interactions., *J. Chem. Phys.*, 2010, **133**, 224701.

59 C. T. Campbell, ATOMIC AND MOLECULAR OXYGEN ADSORPTION ON Ag(ll1), *Surf. Sci.*, 1985, **157**, 43–60.

60 A. Winkler, X. Guo, H. R. Siddiqui, P. L. Hagans and J. T. Yates, Kinetics and energetics of oxygen adsorption on Pt(111) and Pt(112)- A comparison of flat and stepped surfaces, *Surf. Sci.*, 1988, **201**, 419–443.

61 C. T. Campbell, G. Ertl, H. Kuipers and J. Segner, A molecular beam study of the adsorption and desorption of oxygen from a Pt(111) surface, *Surf. Sci.*, 1981, **107**, 220–236.